

Observation and control of separation from bluff bodies

S. Takagi, N. Tokugawa, *National Aerospace Laboratory*, Chofu, Tokyo 182-8522
H. Yoshida, H. Abe, *Mechanical Engineering Laboratory*, Tukuba, Ibaraki 305-8564
T. Atobe, K. Yamamoto, *National Aerospace Laboratory*, Chofu, Tokyo 182-8522

Pressure drag imposed on two-dimensional bluff bodies was experimentally studied, focusing on investigation of the drag-reduction mechanism why D-shaped cross-sectional model has low drag compared with a circular cylinder as a datum model. For accomplishing this study, direct force measurement, smoke visualization around the models and hot-wire and hot-film measurements were conducted. Experimental results show that drag of the D-shaped cylinder is approximately 35% lower than that of the datum in the range of $Re=2 \times 10^4$ - 10^5 investigated. Comparison of visualized flows near the circular and D-shaped models also shows a large difference. That is, earlier separation from the circular cylinder surface induces strong reverse flow, which is related to the formation of Karman vortices, downstream of the separation point, resulting in wide wake region downstream of the model. Hot-wire and hot-film measurements quantitatively assist the above observation. It is inferred that since the straight back plate of the D-shaped model prevents the reverse flow, there is a possibility of more effective plates for drag reduction. Based on this inference, various low-drag configurations are newly proposed and evaluated. Also, several methods to detect separation are discussed.

1. Introduction

Boundary-layer separation from airfoil at high angle of attack is dangerous due to decrease of lift and increase of drag. At this situation, prevention technique prior to separation or earlier reattachment technique even if separation occurred, is practically required. Although flow separation from bluff bodies is unavoidable, a cross section with low pressure drag is also of practical importance. These issues are common regarding separation.

It is well known that a D-shaped cylinder has lower drag coefficient than that of a circular cylinder (Hoerner, and Kambe). Even though there are theories due to Kirchhoff and Heisenberg, or a semi-empirical theory by Roshko, none of them is enough to explain its drag reduction mechanism.

Recently, Hashiguchi has numerically simulated the flow around a D-shaped model comparing to a circular cylinder with a Reynolds number of 10^4 and showed time-dependent vortex structures around the models. Consequently, in spite of no substantial difference between basic vortex structures and shedding frequencies, it is found that D-shaped cylinder has 20% low drag coefficient compared with that of circular cylinder. It is interpreted as reasons of decreasing of pressure drag that although the pressure minimum in the wake immediately behind the D-shaped model is lower than that of the cylinder, its base pressure is higher. However, drag-reduction mechanism itself still remains elusive.

Thus, the present paper deals with experimental investigations of hydromechanical mechanism in drag reduction. In addition to smoke visualization around the models, quantitative measurements were made with the use of a force balance system, hot-wire and multi-hot-film anemometers. Since the coupling between separated free-shear layers and vortex motions has a strong effect on the base pressure, the flow near separated shear layers was visually examined by a high-speed camera. Based on new knowledge obtained from this investigation, further

low drag body shape is proposed and evaluated. Also for active separation control in near future, several methods to detect separation are discussed.

2. Experimental arrangement

2.1 Wind tunnels

Two wind tunnels were used for the present study. Flow around the model was visualized in the Smoke Wind Tunnel (SWT) at the National Aerospace Laboratory. The SWT is of indraft type, whose test section is two-dimensional and 1m high, 0.1m wide and 1m long. The maximum speed in the test section is a uniform velocity of 30m/s, which corresponds to Reynolds number 1×10^5 , based on the uniform velocity, the fluid viscosity and the characteristic length of 50mm. The other wind tunnel called the Calibration Wind Tunnel (CWT) at NAL consists of return circuits and has a 0.65m high, 0.55m wide 1.5m long test section. The flow speed in the test section is varied from 5m/s to 60m/s, which covers $Re=1.8 \times 10^4$ to 2×10^5 . Typical free-stream turbulence levels of SWT and CWT to the uniform velocity are 0.1% and 0.05%, respectively.

2.2 Models

Figure 1 shows the cross-sectional shape of the models used with the flow going from left to right on the D-shaped model. The characteristic length of the model is identically 50mm and the spanwise length is 100mm for SMT and 550mm for CWT. Each model for force-balance measurements in CWT comprises a middle main body with a length of 447mm and two dummy parts with circular end plates, which sustain two-dimensionality of flow around the model. A gap of less than 1mm between the main and dummy parts is covered with a thin Scotch tape, which is cut by sharp knife in the middle of the gap, seemingly resulting in no gap. All models were horizontally installed at CWT and SWT, except for oil-flow and infrared- temperature measurements to detect flow separation from vertically installed model, which allows optical observation from the sidewall of CWT. Main body of SWT models is made of wood, and models used in CWT are made of brass for drag measurement and of wood for infrared and oil-flow measurements. For further experiments, we prepared three models with different cross sections for SWT and a model (e) for force-balance measurement also as shown in Figure 1.

2.3 Other equipments

Two identical sets of force-balance units (Nitta Model UFS-3015A50) fixed on the rigid frame surrounding the CWT test section were used. Though each unit allows six-component measurement, drag force in the flow direction was measured in the capacitance of 22.7kgN with 0.2% accuracy in full scale. Shedding frequency of Karman vortex behind the model was measured by means of a single hot-wire anemometer. A multi-hot-film sensor array aligned 2.5mm apart was wrapped on the circular and D-shaped models of SWT to sense flow separation from instantaneous shear-stress fluctuations, which are uncalibrated. A tiny microphone tip (Knowles Model EM-3368) sensing static pressure fluctuations was installed inside the other identical SWT circular model also to detect flow separation. The model was rotated to measure local pressure fluctuations along the circumferential direction. To visualize the flow around models, a high-speed camera (Photron) together with a laser-light sheet was used in SWT and pictures were captured in frames of 4500 per second.

3. Discussion of results

3.1 General properties

Aerodynamic drag on 2-D circular and D-shaped bodies was directly measured in CWT. Figure 2 shows the results, documenting that the drag coefficients of the datum are found to lie in values of 1.2-1.3 as seen in open literatures, while the D-shaped cylinder has approximately 34% lower pressure drag than that of the circular model in the range of $Re = 0.4 \times 10^5$ to 2×10^5 . The result for the D-shaped cylinder is consistent with those obtained by Umazume and Hayashi et al. as shown in the figure. The drag coefficient of D-shaped model tends to be slightly increased as Re number is decreased.

Flow visualization around 2-D bodies was made in SWT. Typical images are compared in Fig. 3. Since the wake behind the circular cylinder is wider than that of the D-shaped cylinder, the flow separation from the circular model occurs at earlier location compared with the D-shaped cylinder. It is also found that the vortex street behind the D-shaped cylinder is formed farther downstream. This is not contradiction with the fact that the difference in pressure drag at between the base and stagnation point is decreased when the vortices with low pressure are formed farther downstream.

Figure 4 shows the Strouhal number S_t of Karman vortex street in the wake behind the circular and D-shaped models. Shedding-vortex frequency of the D-shaped cylinder is approximately 27% higher, suggesting that the D-shaped cross section has much lower pressure drag according to an empirical relation of $S_t = 0.21 C_D^{-3/4}$ or $C_D = 0.594 S_t^{4/3}$ proposed by Hoerner. Figure 5 depicts mean and fluctuating velocity profiles at the streamwise location of $X/D=4$ for the origin at the base of the model at Re number 7.8×10^4 . Now that the velocity defect behind the D-shaped model is small and the overall level of velocity fluctuation is low across the transverse direction compared with the circular model, the pressure drag imposed on the D-shaped body becomes obviously smaller. This result agrees with the aforementioned force-balance measurement and smoke visualization.

3.2 Control for drag reduction

The above experimental investigations documented that a D-shaped cylinder has much better aerodynamic performance in terms of drag than that of a cylindrical body. It was also observed that there is the strong relation between separating free-shear layers and the formation of the vortex street. Roshko made the pressure measurement along the centerline of the wake behind a 2-D flat plate set normal to the uniform-flow direction. His important finding is the pressure minimum located at not the base of the plate but about twice of the plate width downstream, where vortices are being formed. Visualized flow showed the unsteady wake immediately behind a circular cylinder composes of stronger vortex motions accompanying large amplitude oscillation of separating free-shear layers. This oscillation at separation locations leads to strong reverse flow there. It is inferred in view of this point that the straight back of the D-shaped model plays a role of preventing or weakening reverse flow, resulting in a lower pressure drag. Based on this inference, several configurations with additive plates are prepared already as shown in Fig. 1. Prior to force measurements, S_t number was measured in SWT to roughly evaluate pressure drag. The result is shown in Fig. 6. Since S_t number of the model (e) is the highest among all the models, its drag coefficient was evaluated as plotted in Fig. 2. It is the model (e) that has the lowest drag tested.

3.3 Detection of flow separation

Surface oil-flow technique is known to be the reliable method to detect mean separation line. Oil-flow patterns exposed in a constant flow of 15m/s in CWT are compared in Fig. 7. The lines stagnated on the circular

and D-shaped models are located at 73.3° and 81.3° from the stagnation point, respectively, the former of which shows good agreement with observation by Meier et al. used the same technique. The laminar separation is found to occur at earlier front part of the cylindrical body. Ensuingly, this results in formation of wider wake region. Laminar separation is also known to accompany large pressure fluctuations.

Figure 8 shows that the peak in unsteady pressure distribution coincides with the location of the flow separation. This is emphasized by the results of the wall shear stress measurements as shown in Fig. 9. What is important is the separation location coinciding with neither the peak location in unsteady shear-stress distribution nor the minimum location in the steady stress distribution. The corresponding wall shear stress in separation region does not vanish for two reasons. First, the hot-film sensor cannot distinguish between forward and reverse flow. Second, the sensitivity of the film to shear-stress fluctuation is drastically reduced in stagnant regime, although incipient reverse flow is discernible in instantaneous waveforms at 75.6° .

4. Conclusions

The pressure drag of the circular and D-shaped cylinder models was evaluated by using various methods. Consequently, it was confirmed that the drag of the D-shaped cylinder is approximately 34% smaller than that of the circular one in the range of $Re = 1.8 \times 10^4$ to 2×10^5 . A new cross-section shape with smaller pressure drag compared to the D-shaped model was discovered. Last, for active separation control in near future, several methods to detect flow separation were compared.

References

- Roshko, A. On the drag and shedding frequency of two-dimensional bluff bodies, *NACA TN 3169* (1954).
- Hashiguchi, M. et al. On drag and vortex shedding of cylindrical bodies, *Proc. Jpn. Soc. of Fluid Mechanics* (1999).
- Hayashi, S. et al. An experiment on drag and wake of two-dimensional bluff bodies. *Technical Report of Department of Engineering of Kyushu University* (1977).
- Hoerner, H. *Fluid-dynamic drag* (Hoerner Fluid Dynamics, Albuquerque, 1965)
- Kambe, T. Recent findings from computational fluid-dynamics: drag on cylinders, vortex sound and turbulence statistics, *AIAA Paper 99-3704* (1999).
- Meier, H.U. et al. Experimental study of two-and three-dimensional boundary layer separation. *Unsteady Turbulent Shear Flows*, ed. Michel, Cousteix and Houdeville. Springer-Verlag, Berlin (1981).
- Umazume, K. Private communication (2000).

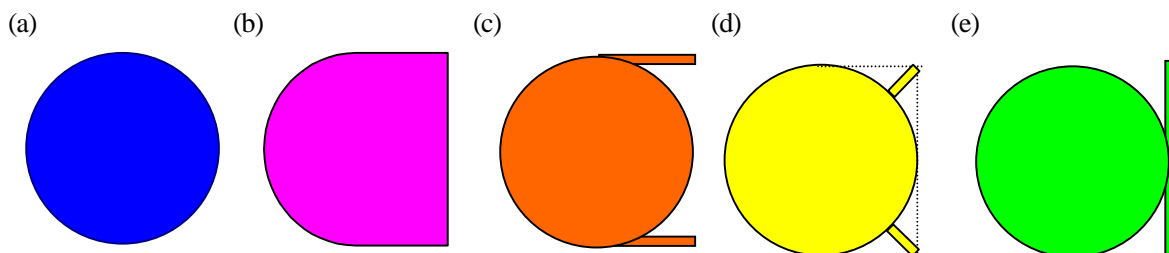


Figure 1. Shape of bluff bodies.

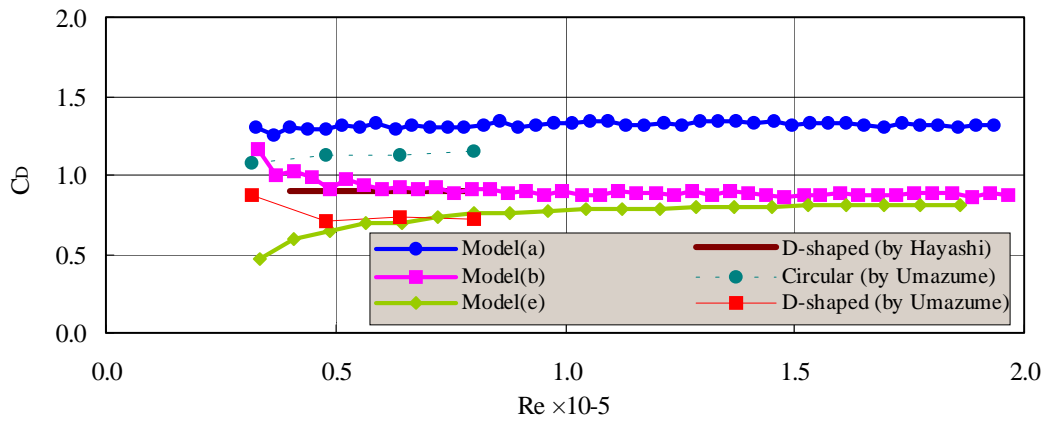


Figure 2. Drag Coefficient C_D vs. Re .

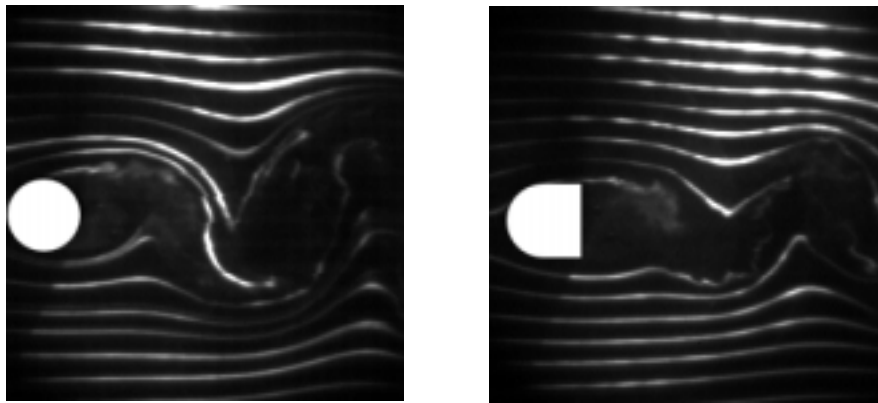


Figure 3. Visualized flow around circular and D-shaped cylinders.

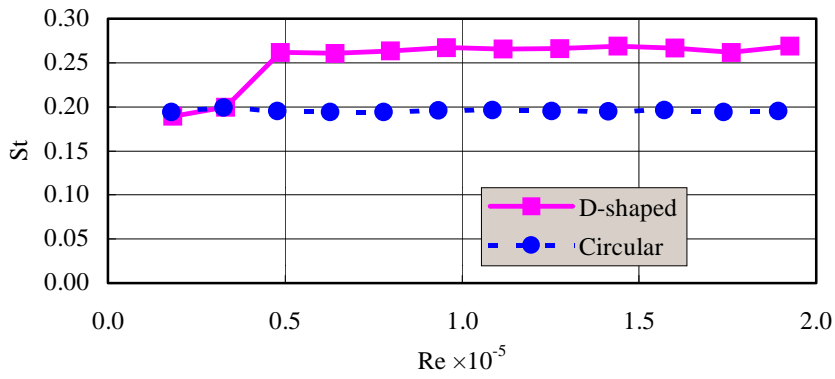


Figure 4. Strouhal number St vs. Re .

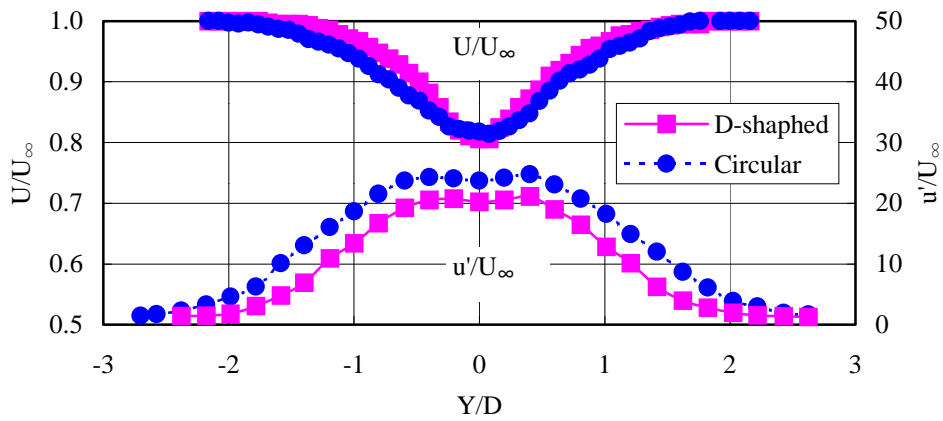


Figure 5. Distributions of mean and fluctuating velocities.

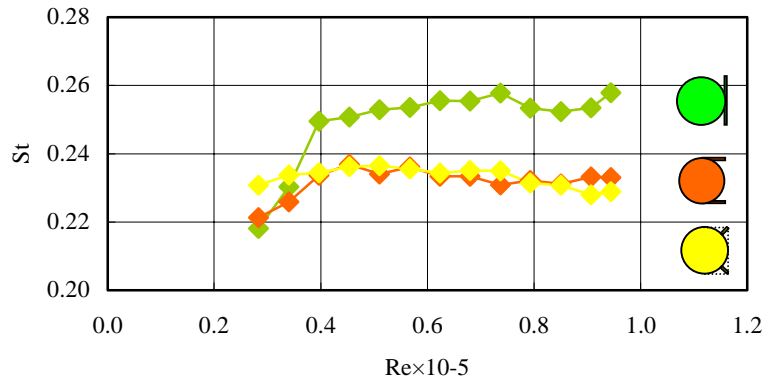
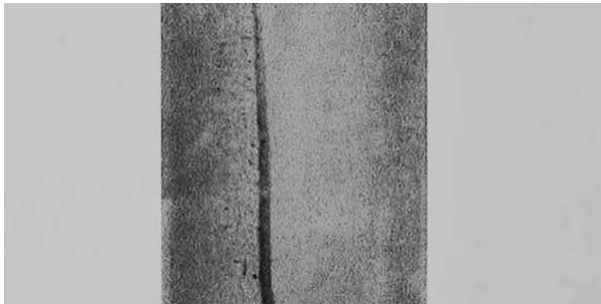


Figure 6. St number of circular bodies with various plates on the leeward side.

(a) Circular cylinder



(b) D-shaped cylinder

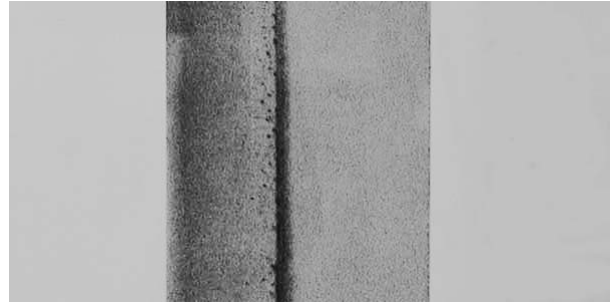


Figure 7. Surface oil flow.

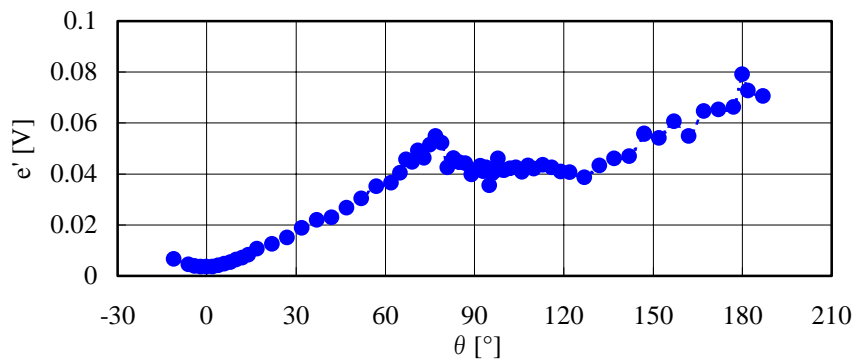


Figure 8. Intensity distribution of unsteady pressure fluctuations along the cylindrical body.

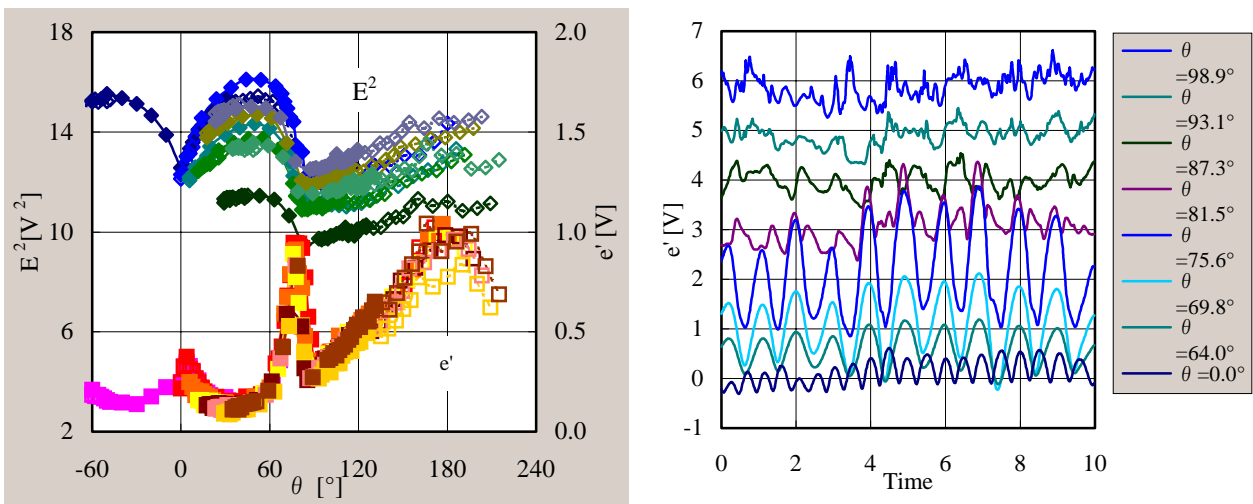


Figure 9. Outputs from hot-film sensor array.